ADVANCED ENERGY MATERIALS
www.advenergymat.de

The Tetrapyrollic Motif in Nitrogen Doped Carbons and M-N-C Electrocatalysts as Active Site in the Outer-Sphere Mechanism of the Alkaline Oxygen Reduction Reaction

*Davide Menga, Jian Liang Low, Ana Guilherme Buzanich, Beate Paulus, and Tim-Patrick Fellinger**

Development and fundamental understanding of precious-group-metal-free electrocatalysts is hampered by limitations in the quantification of the intrinsic activity of different catalytic sites and understanding the different reaction mechanisms. Comparing isomorphic nitrogen-doped carbons, Zn-N-Cs and Fe-N-Cs with the common tetrapyrrolic motif, a catalyst-independent outer-sphere rate-determining step in the alkaline oxygen reduction reaction is observed. Density functional theory (DFT) simulations on tetrapyrrolic model structures indicate the highest occupied molecular orbital (HOMO) level as a good descriptor for the catalytic activity. Contour plots suggest that the electron transfer occurs directly from the tetrapyrrolic coordination site, rather than from the metal center. Metal-free tetrapyrrolic N_4 sites are discovered to be highly active oxygen reduction reaction (ORR) active sites in alkaline that reach turnover frequencies (TOF) of 0.33 and 1.84 s^{-1} at 0.80 and 0.75 V_{RHE} in the order of magnitude of tetrapyrrolic Fe–N_4 sites in the acidic ORR. While Zn-coordination lowers the HOMO level and therefore the catalytic activity, Fe-coordination lifts the HOMO level resulting in TOF values of 0.4 and 4 s^{-1} for tetrapyrrolic Fe–N_4 sites at 0.90 and 0.85 V_{RHE}, respectively. At higher mass activities, the peroxide reduction becomes rate-limiting, where highest peroxide production rates are observed for the nitrogen-doped carbon.

1. Introduction

Carbon-based precious-group metal (PGM)-free electrocatalysts are materials that are intensively studied due to their low cost and application in a wide range of relevant electrochemical reactions.[1] Especially regarding the oxygen reduction reaction (ORR) in proton exchange membrane fuel cells (PEMFCs), they have reached promising initial activity, comparable to state-of-the-art Pt-based electrocatalysts.[2] Even though they are approaching system-relevant stability, they still lack the requirements to meet wide-spread practical application in the technologically more mature acid based PEMFCs.[3] On the other hand, they show exceptional activity and stability in anion exchange membrane fuel cells (AEMFCs), even better compared to Pt-based materials.[4] For this reason, the ORR activity of metal- and nitrogen-co-doped carbons (M-N-Cs) as well as the metal-free nitrogen-doped-carbons (NDCs) is widely studied in alkaline electrolyte and there has been controversial debate on mechanism and the nature of active sites for decades.[5] Generally, there are several differences in the ORR mechanism when the pH increases.[6] In acidic medium, an inner-sphere-mechanism model is generally employed to explain the reduction of O_2 to H_2O_2 or H_2O, with the initial oxidative addition of O_2 to the active metal

D. Menga
Chair of Technical Electrochemistry
Department of Chemistry and Catalysis Research Center
Technische Universität München
Lichtenbergstraße 4, 85748 Garching, Germany
J. L. Low, B. Paulus
Institut für Chemie und Biochemie
Freie Universität Berlin
Arnimallee 22, 14195 Berlin, Germany
A. G. Buzanich
Division 6.3 Structure Analysis
Bundesanstalt für Materialforschung und -prüfung (BAM)
Richard-Willstätter-Straße 11, 12489 Berlin, Germany
T.-P. Fellinger
Division 3.6 Electrochemical Energy Materials
Bundesanstalt für Materialforschung und -prüfung (BAM)
Unter den Eichen 44-46, 12203 Berlin, Deutschland, Germany
E-mail: tim-patrick.fellinger@bam.de

The ORCID identification number(s) for the author(s) of this article can be found under https://doi.org/10.1002/aenm.202400482

DOI: 10.1002/aenm.202400482

center (generally accompanied by a concerted H^+ transfer to the oxygen molecule) proposed as the rate determining step (RDS) for low polarizations.[7] In alkaline environment, in contrast, it has been proposed that both inner- and outer-sphere mechanisms can occur, independently or in parallel.[6b,7c,8] The RDS is generally attributed to the first electron transfer to O_2[9] or the first proton transfer to $*O_2^-$ to form *OOH (* indicates that the intermediate is adsorbed on the active site).[7a,10] Moreover, kinetic isotope effect studies suggest the occurrence of two parallel pathways, one of which has a proton independent RDS.[7c] When an inner-sphere mechanism is taken into account, the possible available adsorption sites in M-N-C are not only the metal centers, but the C atoms close to nitrogen dopants as well. This consideration arises from DFT calculations of the O_2 adsorption on metal-free NDCs (in the Japanese community also referred to as "carbon alloys") completely free from metal sites.[11] While NDCs often show high activity in alkaline medium, high activity in acid is less common for this materials class, sometimes rising concerns of metal impurities.[12] For Fe-N-Cs, Fe poisoning experiments suppress the activity in acidic but not under alkaline conditions, indicating a non-metal-centered active site in alkaline electrolyte, i.e., that ORR might not necessarily happen at the Fe-site.[13] In alkaline electrolyte, the one e^- reduction of O_2 to superoxide ($O_2^{\bullet -}$) is generally reported as a long-range electron transfer happening in the outer Helmholtz plane (OHP) and in most cases promotes only a 2 e^- reduction,[8a] which may however depend on the catalysts porosity influencing the likelihood for a subsequent reaction, let it be inner-sphere or outer-sphere mechanism.[14] Generally, for an outer-sphere charge transfer process, the key factor determining the catalytic activity would be the valence electronic properties, particularly the Fermi energy for the description of the M-N-C as a continuous solid-state catalyst or the energy of the highest occupied molecular orbital (HOMO) for the description of the M-N-Cs by molecular building blocks.[14,15] The relationship between such properties and electrochemical kinetics (i.e., catalytic activity) has been intensively studied,[16] with the majority of related studies discussing them in the context of inner-sphere processes.[17] In a recent DFT study on pyrrolic M-N_4 clusters, the influence of the bound metal species on the HOMO energies was compared among first-row transition metals, providing theoretical support towards the possibility of an outer-sphere mechanism for ORR.[14b]

In order to rationally compare the intrinsic activity of different catalyst via the turnover frequency (TOF), quantifying catalytic parameters such as active-site density (SD) is desirable. For M-N-Cs, these parameters are hard to assess, and different methods have been proposed in the scientific literature. Except for new emerging techniques,[18] the most established methods mostly rely on probe molecules.[19] The use of probe molecules can limit the applicability of the method to ex-situ measurements[19b] or to a certain pH range[19a] and usually requires pre-treatments of the catalytic surface and strict protocols in order to obtain reproducible results.[19a–c] Moreover, so far, no methods are available for NDCs for different N sites, due to the lack of a suitable probe molecule. When assessing SD and intrinsic activity, a catalyst free from inactive side phases is desirable, since these could influence the obtained values by interacting with the probe molecule or by affecting the employed electrochemical method. In our previous work we showed that via an active-site imprinting strategy followed by a transmetalation reaction, Mg-N-C and Zn-N-C containing Mg–N_4 and Zn–N_4 sites respectively can be transformed into active Fe-N-C electrocatalyst without common unfavourable side phases like iron carbide or metallic iron.[20] Moreover, when Zn is employed, tetrapyrrolic metal-coordination sites and hence very active and selective tetrapyrrolic Fe–N_4 sites can be prepared.[21] This synthetic strategy gives the opportunity to obtain a platform to systematically investigate the intrinsic activity of different catalytic sites as well as the reaction mechanism. Very recently, we exploited this methodology in order to assess SD and TOF of an Fe-N-C catalyst with state-of-the-art activity in acidic electrolyte.[22]

In this work, we employ the aforementioned catalyst both in its Zn-coordinating state and in the Fe-coordinating state. After performing a M-to-H^+ ion exchange reaction, different electrocatalysts that differ solely in the type of metal coordinated to the tetrapyrrolic N_4 sites as well as the amount (including the metal-free state) are obtained. The different materials are then measured in a rotating ring disc electrode (RRDE) setup to gain insights into the ORR mechanism and the intrinsic activity of different catalytic sites in alkaline medium.

2. Results and Discussion

The Zn-N-C electrocatalyst is prepared similarly to what was previously reported.[22,23] Briefly, Zn-N-C is prepared by carbonizing 1-ethyl-3-methylimidazolium dicyanamide (Emim-dca) in a $ZnCl_2$/NaCl eutectic mixture (T_m = 250 °C) at 900 °C in Ar atmosphere. Besides having a control on the morphology by simply tuning the mixture composition,[24] the presence of the Lewis-acidic Zn^{2+} ions facilitate the formation of tetrapyrrolic N_4 moieties.[21] The Zn-N-C so obtained is employed in the low- and high-temperature Zn-to-Fe ion-exchange reaction as well as in the M-extraction (i.e., Zn-to-H^+ ion-exchange reaction) in order to obtain the Fe-N-C and the metal-free NDC, respectively. The partially Fe-extracted sample (Fe-N-C-extr) is obtained from the Fe-N-C using aqueous HCl washing, a nonoxidizing acid, and elevated temperatures of 160 °C for 3 d. In order to completely remove the Zn from Zn-N-C and obtain a tetrapyrrolic nitrogen-doped carbon (NDC), the same procedure of aqueous HCl washing was repeated two times. The metal amount in the final catalysts was determined by inductively coupled plasma-mass spectrometry (ICP-MS). Zn-N-C has a Zn content of 0.42 wt% and Fe-N-C has an Fe content of 0.67 wt% before partial Fe extraction and 0.16 wt% after extraction.

Extended X-ray absorption fine structure (EXAFS) measurements are employed to confirm the tetrapyrrolic coordination of the M in the Zn-N-C as well as the Fe-N-C and the partially extracted Fe-N-C. No Zn signal was detected for NDC, further confirming the total extraction of Zn. **Figure 1a–c** shows the magnitude of the Fourier transformed spectrum of the samples, where one main peak at ≈ 2 Å is found, typical for M-N/O scattering in M-N-Cs. When comparing the experimental data with the model based on a 2D tetrapyrrolic Zn-N-C and hydroxy-coordinated Fe-N-C (inset of the figures), a very good agreement is found for Zn-N-C (Figure 1a), Fe-N-C (Figure 1b) and Fe-N-C-extr (Figure 1c), respectively, allowing for the quantitative extraction of structural parameters (Table S1, Supporting Information). Zn cations in Zn-N-C are coordinated to four pyrrolic N at 2.04 Å. In

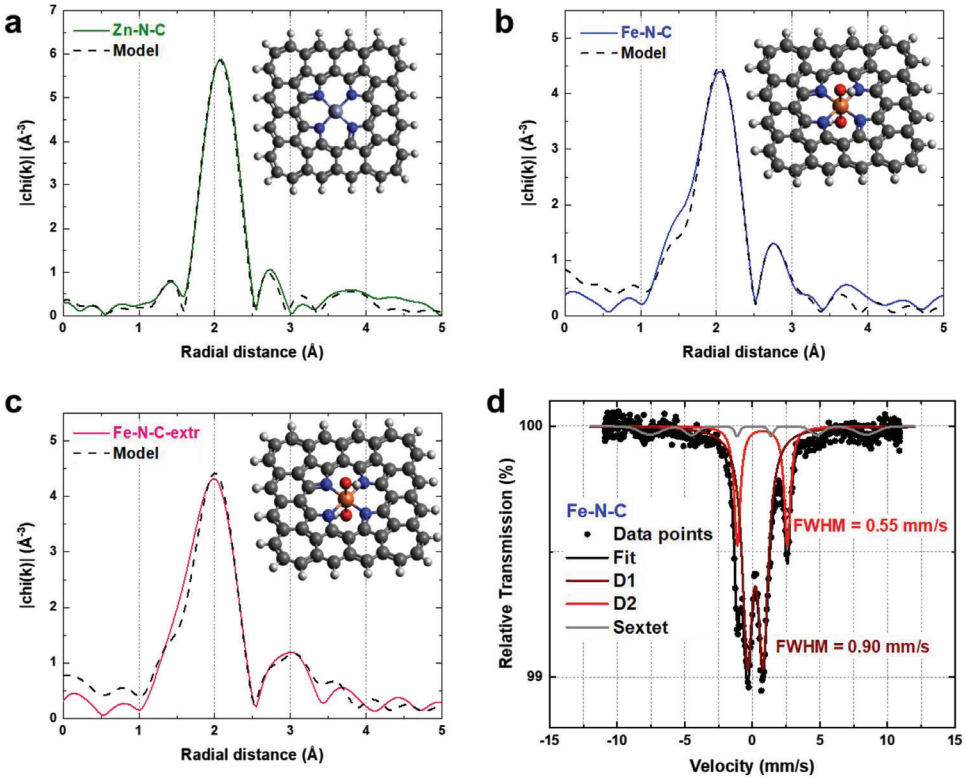

Figure 1. Experimental (phase-corrected) Fourier transform and best fit EXAFS model of the Zn K-edge EXAFS spectra of a) Zn-N-C and Fe K-edge EXAFS spectra of b) Fe-N-C as well as Fe K-edge spectra of c) Fe-N-C-extr to best fit of (b) for comparison. The model used for Zn-N-C is displayed in the inset of (a) and the one used for the two Fe-containing samples is shown in the inset of (b) (Light blue = Zn; orange = Fe; blue = N; red = O; gray = C; white = H). d) Mössbauer spectrum of Fe-N-C measured at 4.2 K; FWHM refers to the line width of the indicated quadrupole doublet.

Fe-N-C, Fe cations are coordinated to four pyrrolic N at 2.05 Å and ≈ 1 O atoms (from OH groups) at 1.84 Å. Fe-N-C-extr shows similar Fe coordination, indicating the same Fe environment of the remaining Fe atoms after extraction (Figure S1 and Table S1, Supporting Information). Cryo-Mössbauer spectroscopy was employed on Fe-N-C to further confirm the environment around the Fe atoms.[25] The spectrum measured at $T = 4.2$ K shows two quadrupole doublets, herein abbreviated as D1 and D2, assigned to atomically dispersed Fe-N_4 sites (Figure 1d), confirming the results obtained via EXAFS analysis. The first doublet, with an isomer shift (IS) of 0.22 mm s^{-1} and a quadrupole splitting (QS) of 1.7 mm s^{-1} is assigned to Fe^{3+} and therefore points to OH/O_2 coordinated Fe-N_4 sites. The second doublet (herein referred to as D2) with an IS of 0.74 mm s^{-1} and a QS of 3.71 mm s^{-1} suggests high-spin Fe^{2+}, as in a bare tetrapyrrolic Fe-N_4 site.[26,27]

Notably, D1 and D2 have a very narrow line width of 0.90 mm s^{-1} and 0.55 mm s^{-1} respectively, which points to a high homogeneity of the Fe-N_4 environment.[22] The Fe content in Fe-N-C-extr is too little to allow for a meaningful deconvolution of the Mössbauer spectrum (Figure S2, Supporting Information).

RRDE measurements were employed to measure the ORR activity of the four isomorphic catalysts in O_2-saturated 0.1 M NaOH electrolyte. For all the measured catalyst a relatively low loading of 0.145 mg cm^{-2} was employed to minimize the chance for artifacts.[28] **Figure** 2a,b shows the Tafel plots and peroxide yield, respectively, and the mass activity values are reported in **Table** 1. Zn-N-C shows the lowest performance and an increase in activity is observed when Zn is removed from the catalyst. This indicates a negative impact on the activity of Zn^{2+} coordinated to tetrapyrrolic N_4 sites and is in agreement with our previous study by Petek et al.[29] Interestingly, the NDC clearly shows an increased peroxide detection in the ring current at lower potentials at a loading of 0.145 mg cm^{-2}, reaching a maximum of 35% at 0.6 V_{RHE} which is more than double of Zn-N-C (15%) (Figure 2b). This will be further discussed later in the manuscript. Since removal of Zn ions from Zn-N-C exposes tetrapyrrolic N_4 sites without changing morphological properties of the material, the change in kinetic current of the two samples related to the reduced Zn content, allows for the determination of the intrinsic activity of tetrapyrrolic N_4 sites in alkaline electrolyte. In our recent work,[22] we suggested that it is possible to calculate the TOF without quantification of the total utilizable SD with the help of a controlled extraction step. Since the extracted amount of metal accounts for removed utilizable active sites (ΔSD), it can be related to the loss in catalytic activity (Δi_{kin}) in Equation (1), giving the TOF value.

$$\mathrm{TOF}\ \left(\mathrm{s}^{-1}\right) = \frac{\Delta i_{kin}\ \left(\mathrm{A\ g}^{-1}\right)}{F\ \left(\mathrm{A\ s\ mol}^{-1}\right) \times \Delta \mathrm{SD}\ \left(\mathrm{mol\ g}^{-1}\right)} \quad (1)$$

where Δi_{kin} represents the difference in the kinetic current between the pristine sample and the extracted sample and ΔSD is the corresponding difference in active-site density, calculated from the amount of extracted metal. To calculate the TOF value

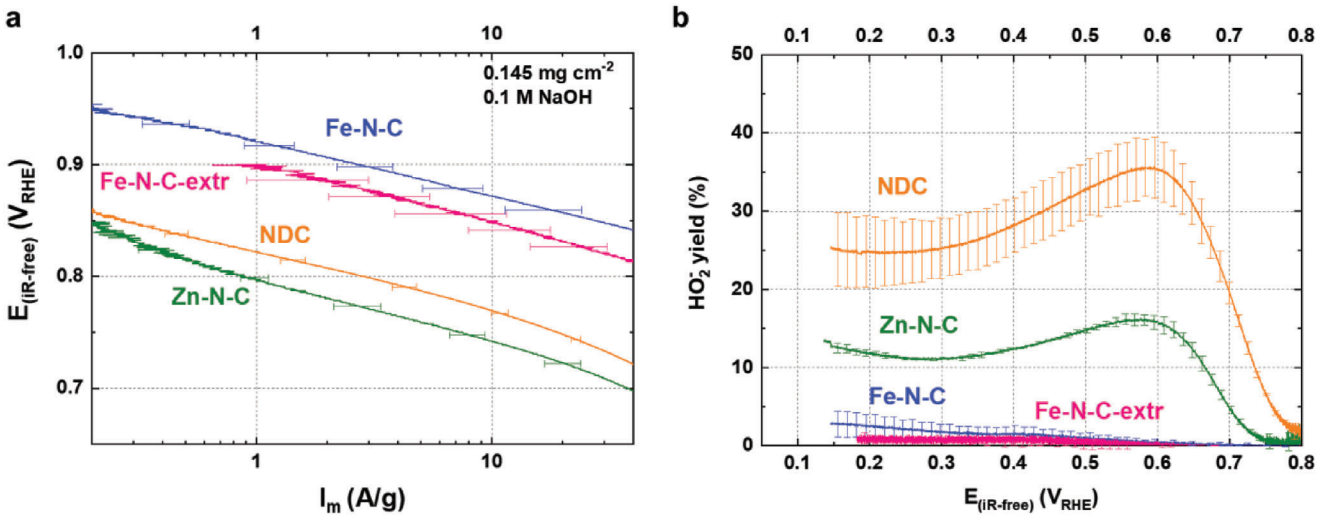

Figure 2. Tafel plots displaying the kinetic mass activity corrected for a) mass-transport limitation. HO_2^- yield obtained via RRDE experiments for b) the four isomorphic catalysts. Measurements were performed at room temperature in O_2-saturated 0.1 M NaOH at 1600 rpm, 10 mV s^{-1} (anodic scans).

for tetrapyrrolic N_4 sites within the NDC catalyst, the ΔSD is calculated from the Zn content of Zn-N-C compared to the Zn-extracted NDC (Table S2, Supporting Information). Noticeable, TOF values of 0.33 s^{-1} and 1.84 s^{-1} are herein calculated for the ORR activity of tetrapyrrolic N_4 sites in alkaline media at 0.80 V_{RHE} and 0.75 V_{RHE}, respectively. The TOF values of tetrapyrrolic N_4-sites in alkaline medium are therefore in the same order of magnitude (even slightly larger) than TOF values of tetrapyrrolic Fe-N_4 sites in the acidic medium.[22]

Moving to the Fe-containing samples, Fe-N-C presents a mass activity of 2.8 ± 0.8 A g^{-1} and 28 ± 10 A g^{-1} at 0.90 V_{RHE} and 0.85 V_{RHE}, respectively, which places this catalyst among the best ORR catalysts reported so far in alkaline electrolyte.[19b,30] The catalyst has a TOF of 0.4 s^{-1} and 4 s^{-1} at 0.90 V_{RHE} and 0.85 V_{RHE}, respectively, which are among the highest values reported for Fe-N-C electrocatalysts in alkaline medium.[18b,19b,c] These values are also in line with reported values obtained with well-established methods,[19b] supporting the validity of the described procedure. Although the removal of Fe in Fe-N-C-extr results in a decreased activity compared to Fe-N-C, both catalysts produce a negligible amount of HO_2^- (<3%) at this catalyst loading (Figure 2b), pointing to a 4 e^- reduction (either direct or apparent) of the O_2 for the Fe-N-Cs. This is clearly different compared to Zn-N-C and NDC, which both produce significant amounts of HO_2^-. Apparently, for both catalysts the 2 e^- reduction has a strong contribution on the ORR activity, curiously even more for the NDC, despite the generally higher activity compared to the Zn-N-C.[9,31]

Table 1. Mass activity (i_{kin}) values at different potentials obtained from RDE measurements in alkaline electrolyte.

Sample	i_{kin} [A g^{-1}]		
	0.90 V_{RHE}	0.85 V_{RHE}	0.80 V_{RHE}
Zn-N-C	–	–	0.9 ± 0.2
NDC	–	–	2.9 ± 0.3
Fe-N-C	2.8 ± 0.8	28 ± 10	153 ± 45
Fe-N-C-extr	1.1 ± 0.7	10 ± 5	67 ± 28

Intriguingly, all tetrapyrrolic catalysts show an identical Tafel slope of TS ≈ 50 mV dec^{-1} between 1 and 10 A g^{-1} (Figure 2a), pointing to an identical rate-determining step in the ORR mechanism for the different active-sites. The observed order of activity is Fe-N-C > Fe-N-C-extr >> NDC > Zn-N-C. This is in stark contrast to the acidic medium, where the Tafel slopes are very different from each other in this current range and the order of activity is Fe-N-C > Fe-N-C-extr >> Zn-N-C > NDC (Figure S3a and Table S3, Supporting Information). The independence of the rate-determining step on the presence and nature of metal-ion sites for otherwise isomorphic catalysts in alkaline electrolyte suggests an outer-sphere mechanism, in which electrons are transmitted over long-range without the need for oxygen adsorption. Rather, the electronic properties of the catalysts must be considered. It has been shown that for outer-sphere electron transfers, the position and electronic structure of the Fermi level and the density of states around it relates to the catalytic activity.[16c,e] In the case of NDCs, the nitrogen doping causes the material to behave as a semiconductor and materials with higher carrier concentration and flat band potential were shown to require lower overpotential to start the ORR.[16c] To explain the observed activity trend, we therefore simulated the electronic properties of NDC, Zn-N-C and Fe-N-C for both periodic and cluster models, representing the description of the catalysts as continuous solid-state materials or by their molecular building blocks (Table S4, Supporting Information).[14a] We performed DFT calculation employing models featuring different pyrrolic-type N_4 coordination sites,[32] namely the metal free H_2N_4, the Zn- and Fe- coordinated M-N_4, resembling NDC, Zn-N-C and Fe-N-C respectively (Figures S4 and S5, Supporting Information). Due to the high pH in alkaline electrolyte, an important role of OH^- adsorption, causing a strong double layer effect and adsorption to metal centers may contribute.[6b] Therefore, we considered the

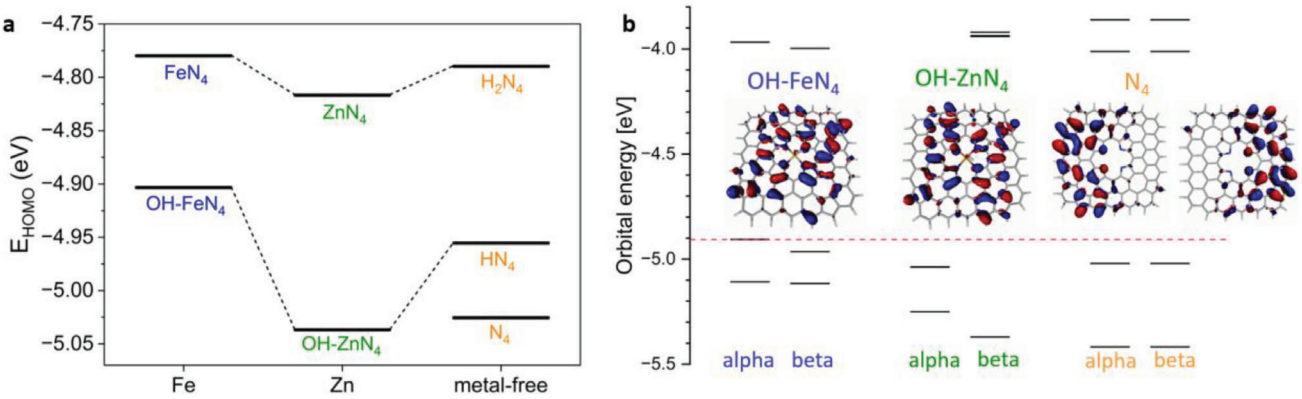

Figure 3. a) HOMO energies of pristine FeN_4, ZnN_4 and H_2N_4 and corresponding OH-bound/deprotonated structures to account for the alkaline environment. b) Frontier molecular orbital diagram OH-FeN_4, OH-ZnN_4 and doubly deprotonated N_4 and the isocontour plot of the corresponding HOMO(s). The red dashed line indicates the HOMO energy of OH-FeN_4. Electronic structures were obtained with PBE0-D3(BJ)/def2-TZVP and COSMO solvation model.

electronic structures of the OH-adsorbed M-N_4 and deprotonated H_2N_4 for the study as well. For the molecular systems, an analogue to the energy of the Fermi level as a descriptor for outer-sphere electron transfer is the energy of the highest occupied molecular orbital (HOMO) depicted in **Figure 3**. From Figure 3a, we observed that the HOMO energies E_{HOMO} of Fe-N_4, Zn-N_4 and H_2N_4 already qualitatively follow the measured reactivity trend in Figure 2a. The trend is retained when the alkaline environment is taken into consideration (OH-FeN_4 vs OH-ZnN_4 vs HN_4), albeit with more pronounced differences in E_{HOMO}. In fact, the shift of 0.13 V in the experimental Tafel plot between Fe-N-C and Zn-N-C (Figure 2a) is in very close agreement with the difference in HOMO energy between OH-FeN_4 (−4.90 eV) and OH-ZnN_4 (−5.04 eV), indicative of an RDS involving a one-electron transfer between the tetrapyrrolic active sites and the oxygen molecules over relatively long-range without the necessity for oxygen adsorption. For the periodic models shown in Figure S5 (Supporting Information), a similar but less quantitative trend is observed among the Fermi levels E_f of OH-FeN_4, OH-ZnN_4 and HN_4. For the NDC, the description is complicated by the degree of deprotonation of the H_2N_4 site in the alkaline medium. Studies on molecular porphyrin compounds determined the average pK_a of the H_2N_4 to be significantly lower than that of water and could even be doubly deprotonated by weaker bases than hydroxides.[33] Due to the larger extent of electron delocalization in NDC, the protons at the H_2N_4 site are expected to be acidic and thus susceptible to deprotonation in the alkaline environment. Among the cluster models, the calculated HOMO energies of HN_4 (−4.96 eV) and N_4 (−5.03 eV) are both intermediate to OH-FeN_4 and OH-ZnN_4, in good agreement with reactivity trend observed in the reactivity in alkaline ORR (Figure 2a). In particular, the E_{HOMO} of the fully deprotonated N_4 is closer to the expected value based on the shifts in the onset potentials, suggesting that it constitutes most of the metal-free N_4 sites. The contour plots of the HOMOs shown in Figure 3b and the element-specific electronic distribution of the HOMO (Table S4, Supporting Information) further suggests that the metal in the M-N_4 site is not likely to be directly involved in the outer-sphere electron transfer, but only influences the reactivity by shifting the HOMO energy, possibly explaining why Fe-N-Cs are able to resist poisoning experiments in alkaline ORR. The absence of the chemical interaction between catalyst and substrate in the RDS at higher potentials in alkaline electrolyte suggests that the coordination site geometry has a substantial impact on the catalyst activity by defining its electronic properties. The well-defined tetrapyrrolic active site structure in pyrolytic Zn^{2+} template-ion reaction derived electrocatalysts allow for a comprehensive electrochemical and theoretical description of the ORR process in alkaline electrolyte.

The abovementioned good fit quality of the XAS analysis and the low line width of the Mössbauer spectra indicate a homogeneous active site geometry. Further, the good quantitative fit between experimental and theoretical results indicate that the tetrapyrrolic coordination site (in contrast to the metal ion) is indeed the active motif from which electrons are emitted, which may explain the very high activity of the Fe-N-C with a high local density of states at the Fermi level. Similarly, the high TOF value for the tetrapyrrolic N_4-site explains the high ORR activity of the NDC. This site has previously not been considered as active site for nitrogen-doped carbons and may explain the activity of previously reported catalysts involving "ORR-inactive" metals.

While similar Tafel slopes are observed for all catalysts in the upper potential range, the Tafel slopes for NDC and Zn-N-C increase to above TS ≈ 120 mV at lower potentials (Figure S3b, Supporting Information). For NDC this is observed at ≈0.77 V and for Zn-N-C at around ≈0.75 V versus RHE. Those potentials represent the onset potentials of the previously mentioned HO_2^- formation. The trend of the peroxide formation is Fe-N-C ≈ Fe-N-C-extr << Zn-N-C << NDC, the inverse of the trend of the ORR activity in acidic electrolyte. Trend and Tafel slopes indicate that here an inner-sphere HO_2^- reduction mechanism becomes rate-determining first for the NDC, then for the Zn-N-C, while the tetrapyrrolic Fe-N-C remains to have a high peroxide reduction activity. The results suggest that the peroxide reduction may occur via inner-sphere mechanism.[14] This picture matches very well with the activity of NDC, which produces high amounts of HO_2^-, since the initial outer-sphere oxygen reduction mechanism will promote mostly the 2 e^- reduction.[8a] When a metal ion is coordinated to the tetrapyrrolic N_4 site, a lower HO_2^- yield

is observed. This effect is particularly pronounced in the Fe-based samples, where even a minute Fe amount is enough to bring the peroxide yield almost to zero. For Fe-N-Cs it has been reported that peroxide reduction in alkaline electrolyte is kinetically favored and that any peroxide intermediate formed during ORR is immediately reduced further to OH^-.[8a]

3. Conclusion

In conclusion, the intrinsic ORR activities of tetrapyrrolic NDCs and the respective Zn- and Fe-coordinated isomorphic Zn-N-C and Fe-N-C electrocatalysts were evaluated in alkaline electrolyte using an RRDE setup in combination with a novel extraction method. Metal-free tetrapyrrolic N_4-sites were found to be highly active, with TOF values in alkaline comparable to TOF values of tetrapyrrolic Fe-N_4 sites in acidic electrolyte.

Independent of the catalysts, a general outer-sphere rate-determining step in the reaction mechanism at mass activities between 1 and 10 A g^{-1} was observed. The experimentally found activity trend of Fe-N-C > NDC > Zn-N-C is matching the calculated electronic properties of tetrapyrrolic model structures. An earlier onset of reaction quantitatively relates well to higher HOMO energy levels, dictated by the state of coordination in the order Fe-N_4 > N_4 >Zn-N_4. Contour plots of all tetrapyrrolic clusters however suggest that the electron transfer occurs directly from the tetrapyrrolic coordination site, rather than from the metal center. The active sites therefore seem to be the same in all investigated catalysts, the activity however depends on their electronic state, dictated by the type of coordination. Noncoordinated tetrapyrrolic N_4 sites reach turnover frequency values of 0.33 s^{-1} and 1.84 s^{-1} at 0.80 V_{RHE} and 0.75 V_{RHE}. While Zn-coordination lowers the HOMO level and therefore the catalytic activity, Fe-coordination lifts the HOMO level resulting in TOF values of 0.4 s^{-1} and 4 s^{-1} for tetrapyrrolic Fe-N_4 sites at 0.90 V_{RHE} and 0.85 V_{RHE}, respectively. The high TOF translates into high mass activity of the Fe-N-C, i.e., 2.8 ± 0.8 A g^{-1} and 28 ± 10 A g^{-1} at 0.90 V_{RHE} and 0.85 V_{RHE}, respectively, ranking this catalyst between the best reported so far in alkaline electrolyte. Because of the independence of the Tafel slope from the metal coordinated to the tetrapyrrolic N_4 sites (including the metal free NDC), the RDS at high potentials is to be found in the first 2 e^- reduction. At higher mass activity the tetrapyrrolic NDC shows selectivity for the 2 e^- reduction of O_2 to HO_2^-, while the coordination of both, Fe or Zn to the tetrapyrrolic N_4 coordination site reduces the peroxide formation. This is likely due to inner-sphere HO_2^- adsorption to the M sites and further reduction to OH^- (for a total of 4 e^-) in the case of M-N-Cs.

4. Experimental Section

Preparation of Zn-N-C: The catalyst was prepared similarly to what previously reported.[22] 1 g of 1-ethyl-3-methylimidazolium dicyanamide (Emim-dca) were thoroughly mixed with 8.26 g of $ZnCl_2$ and 1.74 g of NaCl inside an Ar-filled glovebox. The mixture was then transferred inside a crucible made of alumina and covered with a quartz lid. This was placed inside a tube furnace under constant Ar flow and heated up to a temperature of 900 °C for 1 h, employing a heating rate of 2.5 °C min^{-1}. The final powder was ground in an agate mortar and washed with 0.1 M HCl overnight. After filtering and washing with deionized water in order to reach neutral pH, the sample was dried at 80 °C.

Preparation of Fe-N-C: As previously reported,[21,22] the Zn-to-Fe ion exchange was carried out at low and high temperature. Firstly, Zn-N-C was degassed at 250 °C under vacuum and transferred inside an Ar-filled glovebox. Here, it was mixed with a $FeCl_3$/LiCl eutectic mixture and placed inside a closed Ar-filled flask. After heating the mixture at 170 °C for 5 h, the sample was let to cool down to room temperature, opened to air and washed with deionized water to remove the salt mixture. Afterward, it was stirred in 0.1 M HCl for several hours, filtered, washed with deionized water until neutral pH was reached and dried at 80 °C. The obtained powder was placed again in an alumina crucible and pushed inside a tube furnace pre-heated at 1000 °C under Ar atmosphere. After 15 min, the furnace was turned off and opened to achieve a quick cool down of the sample.

Preparation of NDC: The metal free sample (NDC) was obtained from Zn-N-C after Zn removal (Zn-to-H^+ ion-exchange reaction). Zn-N-C was placed inside a closed Carius tube and stirred for 3 d in 2.4 M HCl at 160 °C. After filtering, thoroughly washing with deionized water and drying, the powder obtained was placed again inside the Carius tube and the entire procedure was repeated a second time in order to achieve the complete extraction of Zn.

Preparation of Fe-N-C-extr: For the partial Fe extraction, Fe-N-C was placed inside a closed Carius tube and stirred for 3 d in 2.4 M HCl at 160 °C. After filtering, washing with deionized water and drying, the final sample was obtained.

Physical Characterizations: X-ray absorption near edge structure (XANES) and extended X-ray absorption fine structure (EXAFS) measurements at the Zn K-edge and at the Fe K-edge were carried out at the BAMline[34] located at BESSY-II (Berlin, Germany), operated by the Helmholtz-Zentrum Berlin für Materialien und Energie. Due to the low metal concentration (<1 wt%) the measurements were performed in fluorescence mode. XANES data evaluation and treatment was performed by using ATHENA program from Demeter package.[35] The further evaluation of the pre-peak analysis was done in Origin, with the Peak Analyser tool, allowing to remove a spline baseline to the pre-peak, and further integrating the resulting area, as shown in Figure S1b (Supporting Information). Phase-corrected (see Supporting Information) EXAFS curves were obtained by convoluting a Hanning-type window to the k-space curves between 1.5 and 10 Å, with a dk = 1. EXAFS curves were Fourier transformed and fitted with a DFT-optimized model adapted from the previous publications[21,22,32] based on a $MN_4C_{96}H_{24}$ cluster (M = Zn or Fe). The model was used to calculate the scattering paths by FEFF to be able to quantify the coordination number and bond-length. The scattering paths to fit both Fe-N-C and Fe-N-C-extr are displayed in Table S1 (Supporting Information). In both cases, an R-range between 1 and 4.5 Å was fitted over, entailing scattering paths until 3.5 Å, and in the latter scattering paths until 3.2 Å. Mössbauer measurements at T = 4.2 K were performed on a standard transmission spectrometer using a sinusoidal velocity waveform with both the source of ^{57}Co in rhodium and the absorber in the liquid He bath of a cryostat. In order to refer the measured isomer shifts to α-Fe at ambient temperature, 0.245 mm s^{-1} was added to the measured values.

Electrochemical Measurements: Rotating ring disk electrode (RRDE) measurements in alkaline electrolyte were performed in a Teflon cell in order to avoid glass dissolution. 0.1 M NaOH was prepared from monohydrate NaOH pellets and deionized ultrapure water. Saturated Ag/AgCl was employed as reference electrode and a Pt wire as counter. Measurements in acidic electrolyte were performed in a three-electrode glass cell using 0.1 M $HClO_4$ as electrolyte, Au wire as the counter electrode and a freshly calibrated RHE as the reference electrode The solution resistance was determined by electrochemical impedance spectroscopy and the reported potentials were corrected accordingly. The ORR polarization curves were corrected for capacitive contributions by subtracting the curves recorded in Ar-saturated electrolyte from the ones recorded in O_2-saturated electrolyte. Catalyst inks were prepared by dispersing 5 mg of catalyst in 1.68 mL of N,N-dimethylformamide and 50 µL of 5 wt% Nafion suspension, followed by sonication. To obtain a catalyst loading of 145 µg cm^{-2}, 10 µL of ink was drop-cast onto a well-polished glassy carbon electrode and dried under an infrared heater for 60 min. For each curve at least two separate measurements were averaged to give the shown polarization curve, and the standard deviation is illustrated with error bars.

Kinetic currents were calculated based on limiting current correction as in reference.[34]

Density Functional Theory (DFT) Calculations: Cluster calculations were performed using the program package TURBOMOLE.[35] The active sites were modeled with the finite-sized $MN_4C_{96}H_{24}$ clusters (M = Fe, Zn, H_2) as shown in Figure S4 (Supporting Information). The hybrid PBE0 functional[36] with Grimme dispersion correction with Becke Johnson damping function D3(BJ) was applied.[37] Geometry optimization was performed with def2-SVP basis while a larger def2-TZVP basis was applied for single-point calculations.[38,39] The conductor-like screening model (COSMO) was applied to describe solvation effects in aqueous environment.[40,41] Electronic steps were converged to 10^{-7} a.u. in the total energy and 10^{-4} a.u. in the orbital energies, while geometric steps were converged to 10^{-3} a.u. in the maximum norm of the Cartesian gradient. Each cluster was calculated with various preassigned multiplicities and the multiplicity that gave the lowest energy was further analyzed. Molecular orbitals were visualized with Molden.[42]

Spin-polarized periodic DFT calculations were performed with the Vienna ab initio Simulation Package (VASP) in the framework of the projector-augmented wave (PAW) method with an energy cutoff of 600 eV.[43] The PBE functional was used with Grimme D3(BJ) dispersion correction with Becke-Johnson damping.[39,44] Hubbard correction for Fe was applied to account for delocalization error associated with the d-electrons ($U = 4$ eV, $J = 1$ eV).[45] The RMM-DIIS algorithm was applied for electronic relaxation with a convergence criterion of 10^{-5} eV. The Gaussian smearing approach with smearing width $\sigma = 0.05$ eV was applied. Ionic relaxation steps were performed with the conjugate gradient algorithm with force convergence of 10^{-2} eV Å^{-1}. K-points were sampled using a $3 \times 3 \times 1$ Γ-centered mesh grid ssduring optimization, and a $6 \times 6 \times 1$ grid for single point calculations. The pyrrolic model as depicted in Figure S5 (Supporting Information) was constructed based on the pyrrolic-D_{4h} model introduced by Menga et al. whereby the carbon lattice is extended to form a periodic 2D lattice with an interlayer vacuum of 15 Å.[21,32]

Supporting Information

Supporting Information is available from the Wiley Online Library or from the author.

Acknowledgements

The German Federal Ministry of Economic Affairs and Energy (BMWi) is acknowledged for funding within the Verbundproject innoKA (Project No.: 03ET6096A). Prof. Hubert Gasteiger is acknowledged for hosting the group and for providing an educative and supportive atmosphere. J.L.L. thanks the Elsa-Neumann Scholarship for funding and the Norddeutschen Verbundes für Hoch- und Höchstleistungsrechnen (HLRN) for computational resources. EXAFS experiments were performed at the BAMline at the BESSY-II storage ring (Helmholtz Center Berlin). The authors thank the Helmholtz-Zentrum Berlin für Materialien und Energie for the allocation of synchrotron radiation beamtime.

Open access funding enabled and organized by Projekt DEAL.

Conflict of Interest

The authors declare no conflict of interest.

Data Availability Statement

The data that support the findings of this study are available from the corresponding author upon reasonable request.

Keywords

atomically dispersed catalysts, M-N-C catalysts, oxygen reduction reaction, PGM free, tetrapyrrolic sites, turnover frequency

Received: January 29, 2024
Revised: June 10, 2024
Published online: July 11, 2024

[1] a) Z. Shi, W. Yang, Y. Gu, T. Liao, Z. Sun, *Adv. Sci.* **2020**, *7*, 2001069; b) T. Asset, F. Maillard, F. Jaouen, in *Supported Metal Single Atom Catalysis* (Eds: P. Serp, D. P. Minh), Wiley, New York **2022**, pp. 531–582; c) A. Kumar, V. K. Vashistha, D. K. Das, S. Ibraheem, G. Yasin, R. Iqbal, T. A. Nguyen, R. K. Gupta, M. Rasidul Islam, *Fuel* **2021**, *304*, 121420.

[2] a) S. Liu, C. Li, M. J. Zachman, Y. Zeng, H. Yu, B. Li, M. Wang, J. Braaten, J. Liu, H. M. Meyer, M. Lucero, A. J. Kropf, E. E. Alp, Q. Gong, Q. Shi, Z. Feng, H. Xu, G. Wang, D. J. Myers, J. Xie, D. A. Cullen, S. Litster, G. Wu, *Nat. Energy* **2022**, *7*, 652; b) A. Mehmood, M. Gong, F. Jaouen, A. Roy, A. Zitolo, A. Khan, M.-T. Sougrati, M. Primbs, A. M. Bonastre, D. Fongalland, G. Drazic, P. Strasser, A. Kucernak, *Nat. Catal.* **2022**, *5*, 311; c) L. Jiao, J. Li, L. L. Richard, Q. Sun, T. Stracensky, E. Liu, M. T. Sougrati, Z. Zhao, F. Yang, S. Zhong, H. Xu, S. Mukerjee, Y. Huang, D. A. Cullen, J. H. Park, M. Ferrandon, D. J. Myers, F. Jaouen, Q. Jia, *Nat. Mater.* **2021**, *20*, 1385.

[3] D. Banham, T. Kishimoto, Y. Zhou, T. Sato, K. Bai, J.-i. Ozaki, Y. Imashiro, S. Ye, *Sci. Adv.* **2018**, *4*, eaar7180.

[4] M. M. Hossen, M. S. Hasan, M. R. I. Sardar, J. b. Haider, Mottakin, K. Tammeveski, P. Atanassov, *Appl. Catal., B* **2022**, *325*, 121733.

[5] H. Chung, G. Wu, D. Higgins, P. Zamani, Z. Chen, P. Zelenay, *Electrochemistry of N4 Macrocyclic Metal Complexes*, Vol. *1*: Energy, 2nd ed., Springer, Berlin, **2016**.

[6] a) R. Sgarbi, K. Kumar, F. Jaouen, A. Zitolo, E. A. Ticianelli, F. Maillard, *J. Solid State Electrochem.* **2021**, *25*, 45; b) S. Rojas-Carbonell, K. Artyushkova, A. Serov, C. Santoro, I. Matanovic, P. Atanassov, *ACS Catal.* **2018**, *8*, 3041.

[7] a) J. Wei, D. Xia, Y. Wei, X. Zhu, J. Li, L. Gan, *ACS Catal.* **2022**, *12*, 7811; b) J. H. Zagal, M. T. M. Koper, *Angew. Chem., Int. Ed.* **2016**, *55*, 14510; c) D. Malko, A. Kucernak, *Electrochem. Commun.* **2017**, *83*, 67.

[8] a) N. Ramaswamy, S. Mukerjee, *J. Phys. Chem. C* **2011**, *115*, 18015; b) N. Ramaswamy, U. Tylus, Q. Jia, S. Mukerjee, *J. Am. Chem. Soc.* **2013**, *135*, 15443.

[9] Y. Wu, S. Nagata, Y. Nabae, *Electrochim. Acta* **2019**, *319*, 382.

[10] X. Li, C.-S. Cao, S.-F. Hung, Y.-R. Lu, W. Cai, A. I. Rykov, S. Miao, S. Xi, H. Yang, Z. Hu, J. Wang, J. Zhao, E. E. Alp, W. Xu, T.-S. Chan, H. Chen, Q. Xiong, H. Xiao, Y. Huang, J. Li, T. Zhang, B. Liu, *Chem* **2020**, *6*, 3440.

[11] a) W. Yang, T.-P. Fellinger, M. Antonietti, *J. Am. Chem. Soc.* **2011**, *133*, 206; b) T. Ikeda, M. Boero, S.-F. Huang, K. Terakura, M. Oshima, J.-i. Ozaki, *J. Phys. Chem. C* **2008**, *112*, 14706.

[12] J. Masa, W. Xia, M. Muhler, W. Schuhmann, *Angew. Chem., Int. Ed.* **2015**, *54*, 10102.

[13] D. Malko, A. Kucernak, T. Lopes, *J. Am. Chem. Soc.* **2016**, *138*, 16056.

[14] a) C. H. Choi, H.-K. Lim, M. W. Chung, J. C. Park, H. Shin, H. Kim, S. I. Woo, *J. Am. Chem. Soc.* **2014**, *136*, 9070; b) J. L. Low, C. Roth, B. Paulus, *J. Phys. Chem. C* **2024**, *128*, 5075.

[15] a) F. Witte, P. Rietsch, S. Sinha, A. Krappe, J.-O. Joswig, J. P. Götze, N. Nirmalananthan-Budau, U. Resch-Genger, S. Eigler, B. Paulus, *J. Phys. Chem. B* **2021**, *125*, 4438; b) R. A. Marcus, N. Sutin, *Biochim. Biophys. Acta* **1985**, *811*, 265.

[16] a) H. Gerischer, R. McIntyre, D. Scherson, W. Storck, *J. Phys. Chem.* **1987**, *91*, 1930; b) H. Gerischer, *J. Phys. Chem.* **1985**, *89*, 4249; c) B. Bera, A. Chakraborty, T. Kar, P. Leuaa, M. Neergat, *J. Phys. Chem. C* **2017**, *121*, 20850; d) P. Szroeder, A. Górska, N. Tsierkezos, U. Ritter, W. Strupiński, *Materwiss. Werksttech.* **2013**, *44*, 226; e) K. K. Cline, M. T. McDermott, R. L. McCreery, *J. Phys. Chem.* **1994**, *98*, 5314.

[17] a) H. Xu, D. Wang, P. Yang, A. Liu, R. Li, Y. Li, L. Xiao, X. Ren, J. Zhang, M. An, *J. Mater. Chem. A* **2020**, *8*, 23187; b) I. S. Amiinu, X. Liu, Z. Pu, W. Li, Q. Li, J. Zhang, H. Tang, H. Zhang, S. Mu, *Adv. Funct. Mater.* **2018**, *28*, 1704638; c) K. Liu, J. Fu, Y. Lin, T. Luo, G. Ni, H. Li, Z. Lin, M. Liu, *Nat. Commun.* **2022**, *13*, 2075.
[18] a) R. Z. Snitkoff-Sol, A. Friedman, H. C. Honig, Y. Yurko, A. Kozhushner, M. J. Zachman, P. Zelenay, A. M. Bond, L. Elbaz, *Nat. Catal.* **2022**, *5*, 163; b) Z. Jin, P. Li, Y. Meng, Z. Fang, D. Xiao, G. Yu, *Nat. Catal.* **2021**, *4*, 615.
[19] a) D. Malko, A. Kucernak, T. Lopes, *Nat. Commun.* **2016**, *7*, 13285; b) F. Luo, C. H. Choi, M. J. M. Primbs, W. Ju, S. Li, N. D. Leonard, A. Thomas, F. Jaouen, P. Strasser, *ACS Catal.* **2019**, *9*, 4841; c) G. Bae, H. Kim, H. Choi, P. Jeong, D. H. Kim, H. C. Kwon, K.-S. Lee, M. Choi, H.-S. Oh, F. Jaouen, C. H. Choi, *JACS Au* **2021**, *1*, 586; d) J. S. Bates, J. J. Martinez, M. N. Hall, A. A. Al-Omari, E. Murphy, Y. Zeng, F. Luo, M. Primbs, D. Menga, N. Bibent, M. T. Sougrati, F. E. Wagner, P. Atanassov, G. Wu, P. Strasser, T.-P. Fellinger, F. Jaouen, T. W. Root, S. S. Stahl, *J. Am. Chem. Soc.* **2023**, *145*, 26222.
[20] a) A. Mehmood, J. Pampel, G. Ali, H. Y. Ha, F. Ruiz-Zepeda, T.-P. Fellinger, *Adv. Energy Mater.* **2018**, *8*, 1701771; b) D. Menga, F. Ruiz-Zepeda, L. Moriau, M. Šala, F. Wagner, B. Koyutürk, M. Bele, U. Petek, N. Hodnik, M. Gaberšček, T.-P. Fellinger, *Adv. Energy Mater.* **2019**, *9*, 1902412.
[21] D. Menga, J. L. Low, Y.-S. Li, I. Arčon, B. Koyutürk, F. Wagner, F. Ruiz-Zepeda, M. Gaberšček, B. Paulus, T.-P. Fellinger, *J. Am. Chem. Soc.* **2021**, *143*, 18010.
[22] D. Menga, A. G. Buzanich, F. Wagner, T.-P. Fellinger, *Angew. Chem., Int. Ed.* **2022**; *Angew. Chem.* **2022**, *134*, 202207089.
[23] K. Elumeeva, N. Fechler, T. P. Fellinger, M. Antonietti, *Mater. Horiz.* **2014**, *1*, 588.
[24] N. Fechler, T.-P. Fellinger, M. Antonietti, *Adv. Mater.* **2013**, *25*, 75.
[25] a) S. Wagner, H. Auerbach, C. E. Tait, I. Martinaiou, S. C. N. Kumar, C. Kübel, I. Sergeev, H.-C. Wille, J. Behrends, J. A. Wolny, V. Schünemann, U. I. Kramm, *Angew. Chem., Int. Ed.* **2019**, *58*, 10486; b) M. T. Sougrati, V. Goellner, A. K. Schuppert, L. Stievano, F. Jaouen, *Catal. Today* **2016**, *262*, 110.
[26] D. Menga, F. E. Wagner, T.-P. Fellinger, *Mater. Horiz.* **2023**, *10*, 5577.
[27] Note that in the Fe-N-C community doublets characteristic for a ferric high-spin are sometimes called D3 rather than D2.
[28] M. Bron, S. Fiechter, P. Bogdanoff, H. Tributsch, *Fuel Cells* **2002**, *2*, 137.
[29] U. Petek, F. Ruiz-Zepeda, I. Arcon, M. Sala, A. Kopac Lautar, J. Kovac, M. Mozetic, D. Menga, M. Bele, T. P. Fellinger, M. Gaberšček, Submitted **2024**.
[30] a) P. G. Santori, F. D. Speck, S. Cherevko, H. A. Firouzjaie, X. Peng, W. E. Mustain, F. Jaouen, *J. Electrochem. Soc.* **2020**, *167*, 134505; b) L. Huo, B. Liu, G. Zhang, R. Si, J. Liu, J. Zhang, *J. Mater. Chem. A* **2017**, *5*, 4868; c) H. Adabi, A. Shakouri, N. Ul Hassan, J. R. Varcoe, B. Zulevi, A. Serov, J. R. Regalbuto, W. E. Mustain, *Nat. Energy* **2021**, *6*, 834; d) K. Yuan, D. Lützenkirchen-Hecht, L. Li, L. Shuai, Y. Li, R. Cao, M. Qiu, X. Zhuang, M. K. H. Leung, Y. Chen, U. Scherf, *J. Am. Chem. Soc.* **2020**, *142*, 2404; e) Z. Jiang, W. Sun, H. Shang, W. Chen, T. Sun, H. Li, J. Dong, J. Zhou, Z. Li, Y. Wang, R. Cao, R. Sarangi, Z. Yang, D. Wang, J. Zhang, Y. Li, *Energy Environ. Sci.* **2019**, *12*, 3508.
[31] Y. Wu, Y. Nabae, *Curr. Opin. Electrochem.* **2021**, *25*, 100633.
[32] J. L. Low, B. Paulus, *Catalysts* **2023**, *13*, 566.
[33] a) S. G. Pukhovskaya, D. T. Nam, Y. B. Ivanova, L. S. Liulkovich, A. S. Semeikin, S. A. Syrbu, M. M. Kruk, *J. Inclusion Phenom. Macrocyclic Chem.* **2017**, *89*, 325; b) A. Farajtabar, F. Gharib, P. Jamaat, N. Safari, *J. Chem. Eng. Data* **2008**, *53*, 350.
[34] A. Guilherme Buzanich, M. Radtke, K. V. Yusenko, T. M. Stawski, A. Kulow, C. T. Cakir, B. Röder, C. Naese, R. Britzke, M. Sintschuk, F. Emmerling, *J. Chem. Phys.* **2023**, *158*, 244202.
[35] B. Ravel, M. Newville, *J. Synchrotron Radiat.* **2005**, *12*, 537.
[36] U. A. Paulus, T. J. Schmidt, H. A. Gasteiger, R. J. Behm, *J. Electroanal. Chem.* **2001**, *495*, 134.
[37] R. Ahlrichs, M. Bär, M. Häser, H. Horn, C. Kölmel, *Chem. Phys. Lett.* **1989**, *162*, 165.
[38] a) J. P. Perdew, M. Ernzerhof, K. Burke, *J. Chem. Phys.* **1996**, *105*, 9982; b) M. Ernzerhof, G. E. Scuseria, *J. Chem. Phys.* **1999**, *110*, 5029.
[39] F. Weigend, R. Ahlrichs, *Phys. Chem. Chem. Phys.* **2005**, *7*, 3297.
[40] a) S. Grimme, J. Antony, S. Ehrlich, H. Krieg, *J. Chem. Phys.* **2010**, *132*, 154104; b) S. Grimme, S. Ehrlich, L. Goerigk, *J. Comput. Chem.* **2011**, *32*, 1456.
[41] A. Klamt, G. Schüürmann, *J. Chem. Soc. Perkin Trans.* **1993**, *2*, 799.
[42] a) G. Schaftenaar, J. H. Noordik, *J. Comput.-Aided Mol. Des.* **2000**, *14*, 123; b) G. Schaftenaar, E. Vlieg, G. Vriend, *J. Comput.-Aided Mol. Des.* **2017**, *31*, 789.
[43] a) G. Kresse, J. Hafner, *Phys. Rev. B* **1993**, *47*, 558; b) G. Kresse, D. Joubert, *Phys. Rev. B* **1999**, *59*, 1758; c) G. Kresse, J. Furthmüller, *Phys. Rev. B* **1996**, *54*, 11169.
[44] J. P. Perdew, K. Burke, M. Ernzerhof, *Phys. Rev. Lett.* **1996**, *77*, 3865.
[45] a) S. L. Dudarev, G. A. Botton, S. Y. Savrasov, C. J. Humphreys, A. P. Sutton, *Phys. Rev. B* **1998**, *57*, 1505; b) A. Allerdt, H. Hafiz, B. Barbiellini, A. Bansil, A. E. Feiguin, *Appl. Sci.* **2020**, *10*, 2542; c) H. Wende, M. Bernien, J. Luo, C. Sorg, N. Ponpandian, J. Kurde, J. Miguel, M. Piantek, X. Xu, P. Eckhold, W. Kuch, K. Baberschke, P. M. Panchmatia, B. Sanyal, P. M. Oppeneer, O. Eriksson, *Nat. Mater.* **2007**, *6*, 516.